Article

Cell Reports

Composite macroH2A/NRF-1 Nucleosomes Suppress Noise and Generate Robustness in Gene Expression

Graphical Abstract

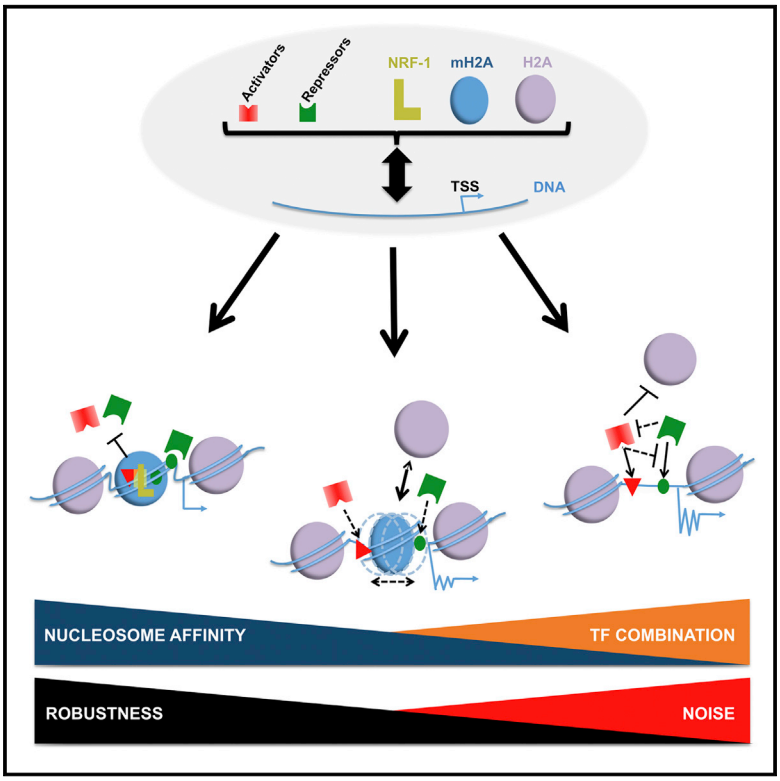

Authors

Matthieu D. Lavigne, Giannis Vatsellas, ..., Marios Agelopoulos, Dimitris Thanos

Correspondence

thanos@bioacademy.gr

In Brief

The histone variant macroH2A marks specific regions in the genome. Lavigne et al. show that a specific subset of promoter-bound macroH2A nucleosomes are stabilized by the transcription factor NRF-1 and reduce the transcriptional variability of target genes.

Highlights

- MacroH2A occupancy generates nucleosome codes for transcription factor access
- MacroH2A nucleosomes are involved in positive and negative control of transcription
- NRF-1 interacts with macroH2A to stabilize and position nucleosomes
- High-affinity promoter-bound macroH2A nucleosomes reduce gene expression variability

Accession Numbers

GSE53133
GSE53103

Lavigne et al., 2015, Cell Reports *11*, 1090–1101
May 19, 2015 ©2015 The Authors
http://dx.doi.org/10.1016/j.celrep.2015.04.022

OPEN ACCESS
CellPress

Cell Reports
Article

Composite macroH2A/NRF-1 Nucleosomes Suppress Noise and Generate Robustness in Gene Expression

Matthieu D. Lavigne,[1,2] Giannis Vatsellas,[1] Alexander Polyzos,[1] Evangelia Mantouvalou,[1] George Sianidis,[1] Ioannis Maraziotis,[1] Marios Agelopoulos,[1] and Dimitris Thanos[1,*]
[1]Biomedical Research Foundation, Academy of Athens, 4 Soranou Efesiou Street, Athens 11527, Greece
[2]Present address: "Alexander Fleming" Biomedical Sciences Research Center, 34 Fleming Street, Vari 16672, Greece
*Correspondence: thanos@bioacademy.gr
http://dx.doi.org/10.1016/j.celrep.2015.04.022

SUMMARY

The histone variant macroH2A (mH2A) has been implicated in transcriptional repression, but the molecular mechanisms that contribute to global mH2A-dependent genome regulation remain elusive. Using chromatin immunoprecipitation sequencing (ChIP-seq) coupled with transcriptional profiling in mH2A knockdown cells, we demonstrate that singular mH2A nucleosomes occupy transcription start sites of subsets of both expressed and repressed genes, with opposing regulatory consequences. Specifically, mH2A nucleosomes mask repressor binding sites in expressed genes but activator binding sites in repressed genes, thus generating distinct chromatin landscapes that limit genetic or extracellular inductive signals. We show that composite nucleosomes containing mH2A and NRF-1 are stably positioned on gene regulatory regions and can buffer transcriptional noise associated with antiviral responses. In contrast, mH2A nucleosomes without NRF-1 bind promoters weakly and mark genes with noisier gene expression patterns. Thus, the strategic position and stabilization of mH2A nucleosomes in human promoters defines robust gene expression patterns.

INTRODUCTION

The biochemical processes that lead to the synthesis of new proteins entail randomness, as they typically involve a small number of diffusing molecules. This can lead to fluctuations in the number of these proteins in a single cell at different times and in different cells of a clonal population. In many cases, this variability can promote transcriptional heterogeneity (noise) in downstream target genes if the fluctuating factor is a transcriptional regulatory protein (Raser and O'Shea, 2005). Furthermore, the inherent ability of transcription factors (TFs) to bind various functional and non-functional DNA sites contrasts with the stereotypic nature of cellular responses, suggesting the existence of cellular mechanisms for noise buffering. Biological systems use a variety of mechanisms to cope with noisy expression to maintain constant expression levels of genes that regulate fundamental functions by resisting endogenous and exogenous perturbations (robustness) (Barkai and Shilo, 2007). Indeed, recent experiments have demonstrated that noise-buffering mechanisms function even under fluctuating conditions and are instrumental in ensuring developmental precision (Ebert and Sharp, 2012; Raveh-Sadka et al., 2012; Spitz and Furlong, 2012; Cheung et al., 2014; Sanchez et al., 2013; Sunadome et al., 2014).

Recent studies in metazoans have shown that the position and/or composition of nucleosomes vary among different cell types, thus contributing to differential regulation of gene expression (Agelopoulos and Thanos, 2006; Schones et al., 2008; Li et al., 2012). Genomic nucleosome positioning is determined by a combination of specific DNA sequences, chromatin remodelers, sequence-specific DNA binding proteins, and modifications in DNA and histones, all of which facilitate entrapment of nucleosomes at specific sites (Choi and Kim, 2009; Sadeh and Allis, 2011; Struhl and Segal, 2013). Sequences occupied by nucleosomes are usually refractory to binding by other factors, which implies that chromatin serves as the template for interpreting the DNA regulatory code that suppresses genetic and/or environmental perturbations and affects phenotypic variation (Cairns, 2009; Jiang and Pugh, 2009; Wang et al., 2011; Iyer, 2012; Luger et al., 2012).

Histone variants contribute to chromatin complexity by creating specialized nucleosomes, which when situated on DNA regulatory elements can have profound effects on nucleosome stability, protein accessibility to DNA, and cellular longevity (Campos and Reinberg, 2009; Talbert and Henikoff, 2010). In contrast to the canonical H2A, macroH2A (mH2A) features a large (~30 kDa) C-terminal macrodomain connected to the H2A-like domain via a short, flexible linker that protrudes from the core nucleosome structure (Pehrson and Fried, 1992; Chakravarthy et al., 2005). Although mH2A proteins are enriched at the inactive X chromosome (Costanzi and Pehrson, 1998), their related function is unclear, as female embryonic stem cells lacking mH2A (Tanasijevic and Rasmussen, 2011) or even mice lacking mH2A1 can inactivate their X chromosome normally (Boulard et al., 2010). Early studies showed that mH2A-containing nucleosomes reside at the promoters and coding regions of repressed genes, suggesting that it plays a general role in repressing gene expression (Angelov et al., 2003; Agelopoulos and Thanos, 2006). Similarly, mH2A variants act as pleiotropic

tumor suppressors, blocking cellular reprogramming by inhibiting the expression of genes involved in pluripotency (Kapoor et al., 2010; Pasque et al., 2011; Gaspar-Maia et al., 2013; Barrero et al., 2013).

Here, we demonstrate that contrary to what was previously believed, lone (singular) mH2A nucleosomes can be found on the promoters of both expressed and non-expressed genes, and play bifunctional (positive or negative) roles in transcriptional regulation. We find that high-affinity, promoter-bound mH2A nucleosomes correlate with the co-binding of nuclear respiratory factor 1 (NRF-1) (Evans and Scarpulla, 1990), and that the strategic positioning of these composite mH2A/NRF-1 nucleosomes within key gene promoters leads to stable and highly specialized chromatin landscapes that provide and/or limit access to subsets of TFs. This mechanism suppresses transcriptional variability and reduces the impact of changes induced either by lowering the levels of mH2A in the cells (genetic perturbation or stochastic fluctuations [intrinsic noise]) and/or by viruses infecting the cells (environmental perturbation [extrinsic noise]). This system is robust because NRF-1 stabilizes nucleosome binding to these promoters via direct protein-protein interactions with mH2A. By contrast, genes lacking mH2A or genes bound with low affinity by mH2A nucleosomes (without NRF-1) show increased variability (higher noise) in expression upon intrinsic or extrinsic perturbation. Taken together, our findings suggest that noise suppression is mediated by robust deterministic mechanisms superimposed on specific DNA sequences that instruct the assembly of highly specialized chromatin landscapes that are refractory to perturbations.

RESULTS

mH2A Nucleosomes Are Enriched at the Promoters of Expressed and Non-expressed Genes

To investigate the functional role of mH2A nucleosomes, we determined their precise genome-wide location in HeLa epithelial and Namalwa B cells by combining micrococcal nuclease (MNase) digestion of native chromatin with immunoprecipitation (N-ChIP), followed by deep DNA sequencing (Umlauf et al., 2004; Zhang and Pugh, 2011). Sharp, single nucleosome mH2A peaks were detected by means of intersecting MACS and QuEST algorithms outputs (see Experimental Procedures). Figures 1A and S1A show that singular mH2A-containing nucleosomes are enriched at promoters (<3 kb upstream of transcription start sites [TSSs]) and regulatory DNase hypersensitive sites (DHSs), especially in Namalwa cells (see Experimental Procedures). A comparison of genomic sites bound by mH2A nucleosomes revealed only a small overlap between HeLa and Namalwa cells (Figure S1B), suggesting a cell-type-specific mH2A nucleosome deposition mechanism. For instance, Figure 1A (bottom) compares UCSC browser snapshots of the same region (promoter or inter-/intragenic) between these cell lines and demonstrates the differences in the mH2A nucleosome localization maps. Consistently, the biological processes associated with the genes bound by mH2A in HeLa cells are fewer and less significant than those in Namalwa cells (Figures S1C and S1D). In Namalwa B cells, the mH2A target genes control a diverse list of genes, suggesting that this histone variant is not associated with specialized biological functions, and instead plays a more general role in a variety of cellular functions (Figure S1D).

We calculated the average binding frequency of mH2A to all annotated transcription units from 1 kbp upstream of the TSS to 1 kbp downstream of the transcription termination site (TTS). We identified two classes of genes bearing high (labeled N656) or medium (N3353) affinity mH2A promoter-bound nucleosomes in Namalwa cells (Figure 1B), whereas we found only a single binding class in HeLa cells (H585; Figure S1E). Next, we divided these genes into quantiles according to their expression levels as determined by RNA sequencing (RNA-seq; see the Supplemental Experimental Procedures) and discovered that the most frequent position of mH2A nucleosomes is immediately upstream of the TSS (dyad axis within −75 bp from TSS) of both expressed and non-expressed genes (Figure S1F). For each expression category, a single line in Figures 1C and S1G represents the average enrichment profiles of mH2A ChIP-seq reads per gene relative to their TSS. Remarkably, we found that the mH2A binding frequencies were slightly higher for the promoters of expressed genes than for the promoters of lower- or non-expressed genes (BOUND, Figures 1C and S1G). By contrast, singular mH2A nucleosomes were rare at regions localized farther upstream or downstream of the TSS (BOUND, Figures 1C and S1G). We confirmed these conclusions by correlating the higher proportion of mH2A-bound genes to higher expression levels (Pearson's $r = 0.958$; Figure 1D). Thus, a highly expressed gene has a greater probability of containing a promoter-bound mH2A nucleosome compared with a low- or non-expressed gene, and/or an mH2A nucleosome has a higher probability of binding to the promoter of an expressed gene than to a low- or non-expressed gene. These findings challenge the current understanding of mH2A function (Buschbeck et al., 2009; Gamble et al., 2010; Changolkar et al., 2010) and suggest that mechanisms exist to ensure precise mH2A nucleosome positioning at promoter regions, which is independent of the respective gene expression level, and that the presence of an mH2A nucleosome at promoters does not predict gene activity.

An important prediction derived from the above findings is that mH2A nucleosomes should coexist with RNA-PolII on expressed genes. Indeed, Figure S1H shows that native mononucleosomes immunoprecipitated with an α-PolII antibody contain mH2A. In agreement with this observation, we found that mH2A nucleosomes also globally overlap active gene marks such as DHSs and are flanked by nucleosomes containing H3K4Me3 (Figure S1I).

mH2A Nucleosomes Restrain the Variability of Transcriptional Programs Induced by Genetic or Environmental Perturbation

To evaluate whether mH2A nucleosomes directly affect transcription, we examined how the average frequency of mH2A nucleosomes binding per gene correlates with variability in differential expression (DE) in cells knocked down for mH2A (genetically perturbed cells) as compared with control cells (see Supplemental Results). First, we investigated the distribution of mH2A nucleosomes in the 1,436 genes (Figures S2C and S2E) that were differentially expressed in Namalwa mH2A knockdown (KD) cells. We generated heatmaps by K-means clustering and

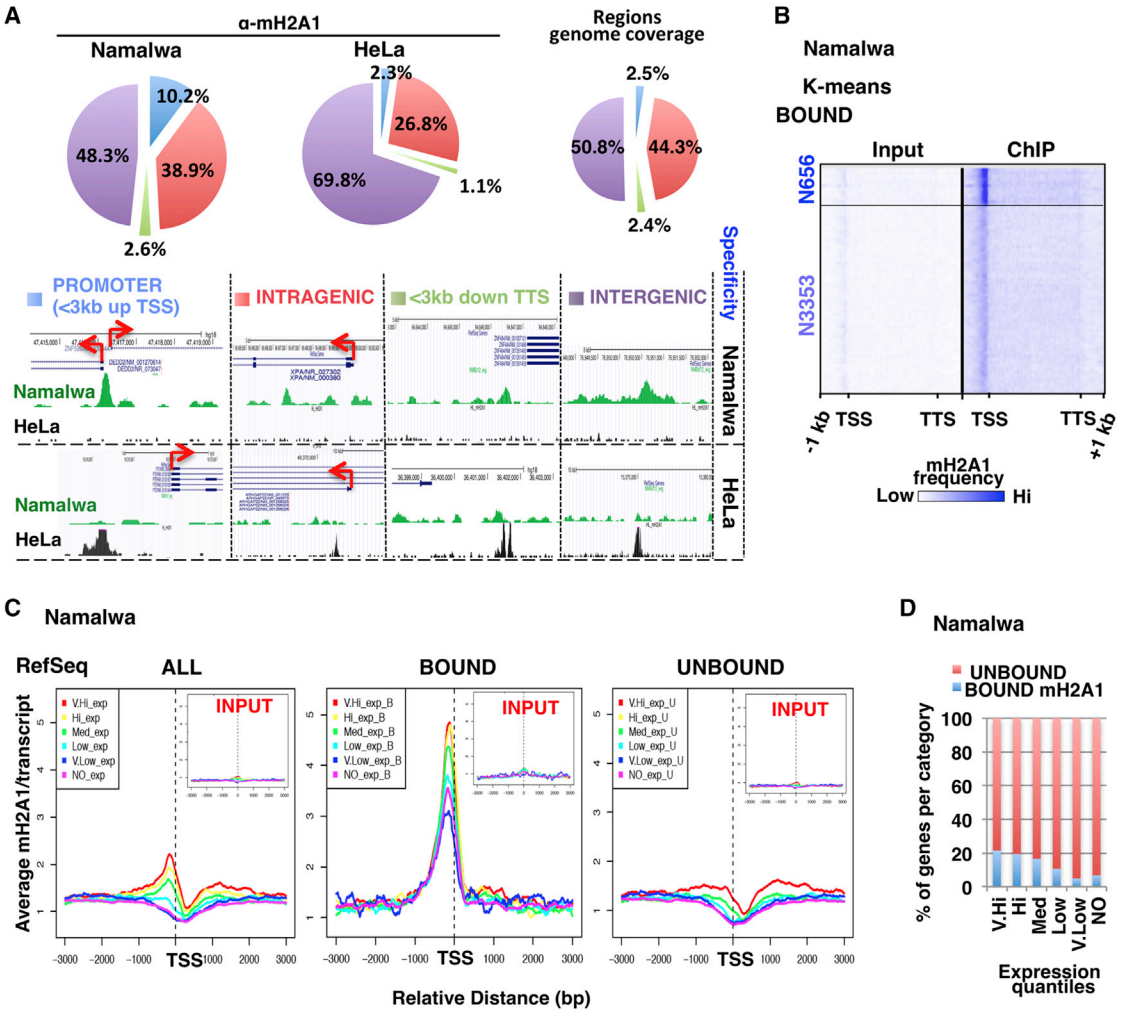

Figure 1. mH2A Nucleosomes Are Enriched at the Promoters of Expressed and Non-expressed Genes

(A) Top: pie charts depicting the genome-wide distribution of mH2A ChIP-seq peaks identified by QuEST and MACS (see Experimental Procedures). The percentage of mH2A peaks within 3 kb upstream of TSSs (PROMOTER in blue) and within 3 kb downstream of TTSs (in green) was determined. The remaining mH2A peaks were divided into intragenic (red) and intergenic (purple) regions. For comparison, the relative percentage of the total genome assignable to each region is also shown (small pie chart on the right). Bottom: ChIP-seq profile snapshots (UCSC browser) of genes bound by mH2A1, depicting the cell-type-specific density profiles of Namalwa (green track) and HeLa (black track) cells (compare top and bottom panels for each corresponding region). Gene models in dark blue depict exons as boxes and introns as lines. Transcript orientation and TSSs are indicated by red arrows.

(B) Heatmap depicting the frequency of mH2A nucleosomes ChIP-seq reads on target genes in Namalwa cells (from −1 kb from TSS to +1 kb from the TTS of RefSeq transcripts). The darker blue color indicates a higher frequency of mH2A1 binding. K-means clustering identified high-frequency (N656) and medium-frequency (N3353) mH2A-bound promoters.

(C) mH2A is located at the TSSs of active and inactive genes. mH2A1 ChIP aggregated enrichment profiles around TSSs in Namalwa cells. All expressed genes were identified by RNA-seq and divided into five groups of equal sizes according to their expression levels (expression quantiles, with ''V.Low_exp'' corresponding to the lowest expression levels and ''V.Hi exp'' corresponding to the highest). The ''NO_exp'' category includes all genes with no detectable expression. Each line represents the average number of reads per transcript plotted relative to the TSS for each expression group. The left diagram (ALL) represents the average number of mH2A1 reads when ALL RefSeq genes are considered. The middle diagram (BOUND) represents the average number of mH2A1 reads if we consider only the bound genes identified in (B). mH2A1 is depleted from the promoters of all expression categories for the UNBOUND genes (not identified in B). The insets depict the INPUT reads.

(D) Bar graph illustrating the correlation between mH2A binding at the TSS and the expression levels for the six categories of genes shown in (C).

See also Figures S1–S5 and Tables S1, S3, and S4.

identified three classes of genes bearing distinct promoter-bound mH2A read densities: high (I-Hi), medium (I-Med), and no (II) mH2A (Figure 2A). Next, for each gene, we examined the effect of mH2A KD on gene expression (Figure 2B). Remarkably, we found an inverse relationship between high-affinity mH2A binding and the target gene fold change (FC) amplitude in mH2A KD cells (I-Hi; Figures 2A and 2B). In other words, promoters with the highest levels of mH2A binding (I-Hi, strong

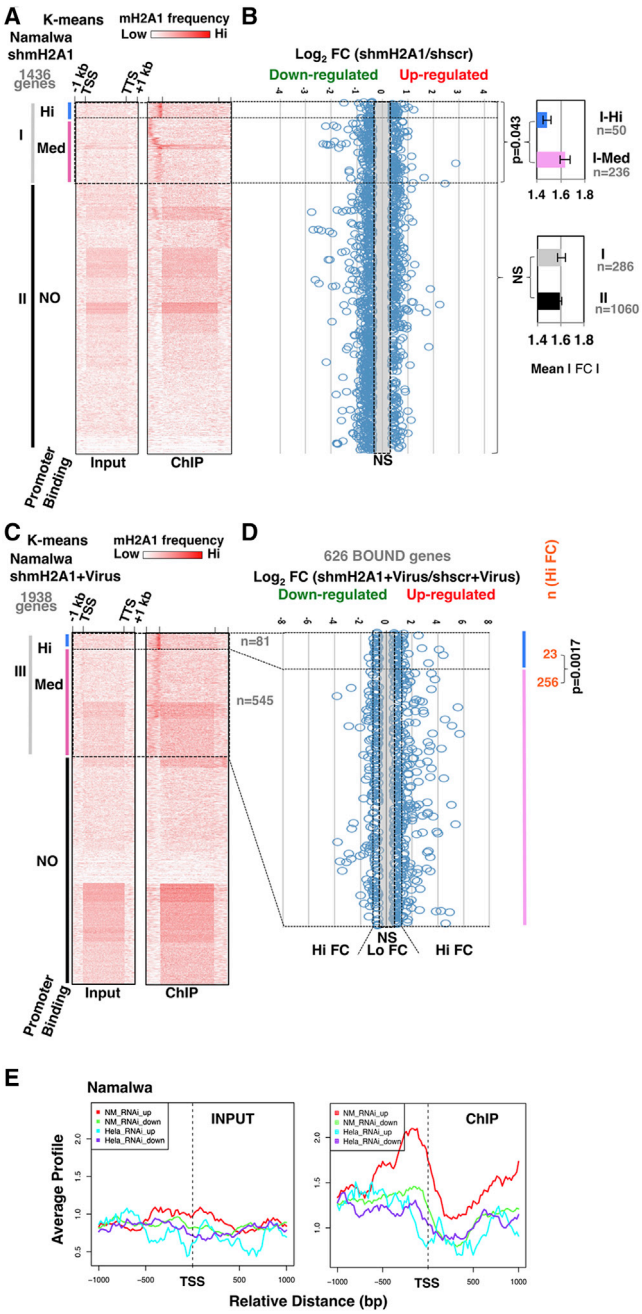

Figure 2. mH2A Nucleosomes Are Direct Bifunctional Regulators of Transcription and Restrict Transcriptional Variability upon Genetic and/or Environmental Perturbations

(A) mH2A1-nucleosome distribution on the 1,436 RefSeq annotated genes that are affected by mH2A KD in Namalwa cells (defined in Figures S2C and S2E). Heatmaps display the density of ChIP-seq (ChIP) and input reads centered on transcription units from −1 kbp from the TSS to +1 kbp from the TTS. The darker red color indicates a higher frequency of mH2A1 binding. K-means clustering highlights the distinct local enrichment for gene promoters bound by mH2A1 (cluster I) with high (I-Hi) or medium (I-Med) frequency or not bound by mH2A1 (cluster II).

(B) Scatterplots illustrating DE (log_2 FC) in mH2A KD Namalwa cells. The genes were sorted on the y axis as defined in (A). The bar graphs on the right demonstrate that the mean |FC| ± SEM is lower for I-Hi compared with I-Med (t test statistic = −1.72, p = 0.043). In contrast, there is no significant difference (t test statistic = 0.35, p = 0.72 [NS]) between directly regulated genes (I-Hi + I-Med) and indirectly regulated genes (II).

(C) Same as in (A) except that the genes examined were the 1,938 genes affected by virus infection in mH2A KD Namalwa cells (defined in Figures S2D and S2E). K-means clustering highlights the distinct local enrichment on promoters bound by mH2A1 (cluster III) with high (III-Hi) or medium (III-Med) frequency or not bound by mH2A1 (NO).

(D) Same as in (B) for cluster III. A chi-square test revealed that there are more genes with Hi FC ($|log_2$ FC| > 1) for cluster III-Med than for cluster III-Hi (chi-square statistic = 9.85, p = 0.0017).

(E) Average mH2A1 ChIP-seq read enrichment profiles around the TSS in Namalwa cells for all RefSeq annotated genes affected by shmH2A1 in either Namalwa or HeLa cells (defined in Figure S2C). The genes were divided into four groups: genes upregulated (NM_RNAi_UP in red) or downregulated (NM_RNAi_DOWN in green) in Namalwa mH2A KD cells or in HeLa mH2A KD cells (Hela_RNAi_UP in turquoise, Hela_RNAi_DOWN in purple).

See also Figure S2 and Tables S2 and S4.

binders) showed a low average absolute gene expression FC in mH2A KD cells (closer to the control baseline). Importantly, this corresponds to lower variability in expression among the genes of this cluster. By contrast, genes bound by mH2A at an intermediate level (medium frequency) displayed a significantly higher average absolute FC (compare I-Med to I-Hi in Figure 2B, t test statistic = −1.72, p = 0.043). As a control, we show that the average absolute expression FC is not significantly different for all the genes bound by mH2A compared with unbound genes (II) (Figure 2B, t test statistic = 0.35, p = 0.72 [NS]), indicating that variability in expression is buffered only in the strong mH2A-bound promoters.

Next, we tested the effect of combined genetic and environmental perturbations on gene expression. We performed K-means clustering on the 1,938 genes affected in virus-infected mH2A KD cells ("combined environmental and genetic perturbations," Figures S2D and S2E) and identified 626 genes (III) bearing promoter-bound mH2A (Figures 2C and 2D). In agreement with the data from uninfected cells (Figures 2A and 2B), we found an even more pronounced inverse relationship between high-frequency mH2A binding (III-Hi) and expression variability from the control baseline in mH2A KD cells (Lo FC, Figures 2C and 2D). Indeed, the average absolute log_2 FC was lower (1.02) for the genes that were more frequently occupied by mH2A1 (III-Hi) than for the less frequently bound genes (III-Med, 1.29; t test statistic = 2.54, p = 0.011). Consistently, we also identified fewer genes with absolute log_2 FC > 1 (Hi FC) in the III-Hi than in the III-Med cluster (chi-square statistic = 9.85, p = 0.0017, Figure 2D). These data suggest that the expression of genes bound by high-affinity mH2A nucleosomes remains remarkably constant upon environmental (virus infection) or genetic (mH2A KD) perturbation, or both. An additional consequence of this mH2A-driven mechanism is that it regulates both the range and the spectrum of the antiviral gene expression program (see Supplemental Results) by prohibiting abnormal transcriptional responses (Figure S6A).

The specificity of our experiments was further demonstrated by the fact that genes affected by mH2A KD contain promoter-bound mH2A nucleosomes in Namalwa cells, as opposed to the genes deregulated by mH2A KD in HeLa cells, which do not contain mH2A nucleosomes in Namalwa cells (compare

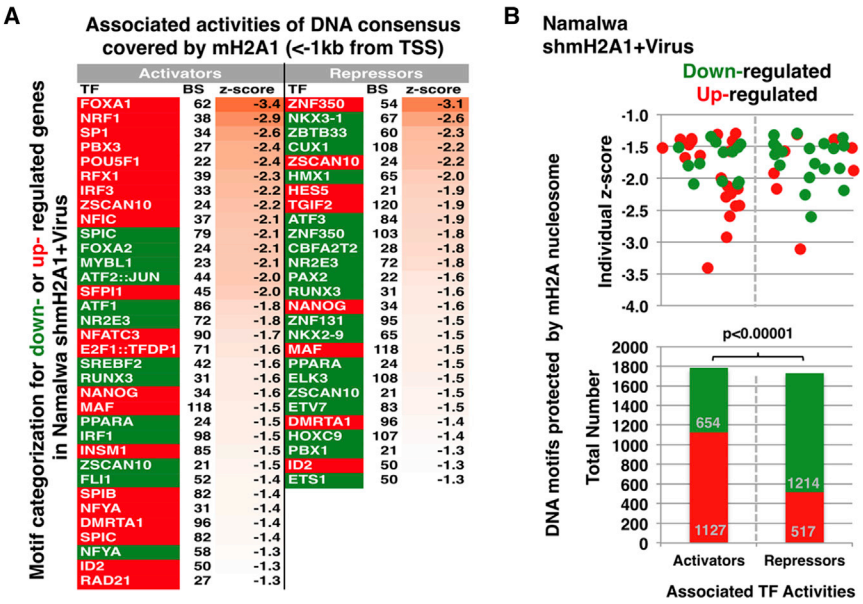

Figure 3. A mH2A Nucleosome Code in Regulation of Transcription

(A) Table displaying the main TF DNA binding consensus motifs corresponding to either activators (left column) or repressors (right column) that were identified within the footprint of the mH2A nucleosomes for genes that were up- or down-regulated (red and green, respectively) in Namalwa KD cells after virus infection (defined in Figure S2D). The values under BS correspond to the number of identified binding sites. The relative enrichment (*Z* score) for each motif is also shown on the right.

(B) Analysis of transcriptional activities associated with DNA motifs masked by promoter-bound mH2A nucleosomes for genes that are up- or downregulated in virus-infected Namalwa mH2A KD cells. Shown at the top is a scatterplot depicting the probabilities calculated for each motif (individual *Z* score) for putative activators (left) and repressors (right). Shown at the bottom is a bar graph depicting the sum of all activator and repressor putative DNA motifs, illustrating a higher proportion of upregulated genes in mH2A KD virus-infected cells when the nucleosome masks activator sites and a reciprocally higher proportion of downregulated genes when the nucleosome masks repressor sites (chi-square test: 393.586, $p < 0.001$).

See also Figure S2 and Tables S2 and S3.

NM_RNAi_UP or _DOWN with HeLa_RNAi_UP or _DOWN in Figure 2E).

mH2A Nucleosomes Print Bifunctional Codes That Instruct TF Access

The unexpected finding uncovered by the mH2A KD transcriptomic analysis was that, in contrast to what was previously believed, mH2A nucleosomes play both a positive and a negative role in transcription (see Figure 2 and Supplemental Results). We hypothesized that they do so by controlling the differential accessibility of activators and repressors to specific regulatory regions. We analyzed the DNA sequences underlying mH2A nucleosomes (Experimental Procedures) and discovered that genes downregulated in mH2A KD cells bear promoter mH2A nucleosomes that tend to mask repressor binding sites (e.g., ZBTB33 and CUX1), whereas genes upregulated in KD cells bear mH2A nucleosomes that mask activator binding sites (e.g., IRF3 and PBX3; Figure 3A). In general, we found a distinct enrichment of activator or repressor TF binding sites (TFBSs) under the footprint of mH2A nucleosomes for genes that are respectively up- or downregulated in virus-infected mH2A KD cells (inverse distribution of TFBS *Z* score and inverted proportional distribution of the number of sites: chi-square test: 393.586, $p < 0.00001$; Figure 3B). Taken together, these findings suggest that mH2A nucleosomes play a direct bifunctional role in positive and negative control of transcription.

NRF-1 Interacts with mH2A Nucleosomes to Confer High-Efficiency Nucleosome Positioning

To examine the mechanisms that govern the differential binding affinity of mH2A nucleosomes for specific promoters, we further analyzed the nature of the DNA sequences bound by mH2A nucleosomes. We identified the most frequently occurring TFBSs that coexist with mH2A nucleosomes in promoters and in the whole genome (Figures 4A and 4B). We found that mH2A nucleosome binding sites most often coincide with putative sites for the bzip TF NRF-1 (Virbasius et al., 1993). Furthermore, and in agreement with our previous observations (Agelopoulos and Thanos, 2006), we showed that mH2A binding sites also overlap with additional bzip protein binding sites such as ATF and CREB, as well as with DNA sites recognized by ETS, E2F, and NFY (Figures 4A and 4B).

To investigate the relationship between NRF-1 and mH2A, we carried out ChIP-seq experiments to determine the genome-wide locations of NRF-1 using our affinity-purified anti-NRF-1 antibody (Figure S4A) and chromatin prepared from crosslinked Namalwa cells. We identified 8,236 NRF1 binding sites, 45% of which were mapped at promoter regions (Figure S4B). Figure 4C depicts the striking similarities between the current NRF-1 consensus sequence (Transfac database) and the most frequent motifs we identified by de novo motif discovery using NRF-1 and mH2A ChIP-seq. These data suggest a high probability for the coexistence of mH2A nucleosomes and NRF-1. Indeed, Figure 4D shows that a substantial proportion (14%) of all mH2A genomic sites are also bound by NRF-1, and that nearly all (91%) of the mH2A sites with an NRF-1 consensus are also bound by NRF-1 in vivo (Figure 4E). These NRF-1 sites usually flank the mH2A-nucleosome dyad axis (±20 bp; Figure 4F), and reciprocally, the average frequency of mH2A-nucleosomes (defined by the coordinates of their dyad axis) is maximal around NRF-1 peak centers (Figure S4C). Together, these data suggest that NRF-1 and mH2A nucleosomes co-occupy the same DNA elements.

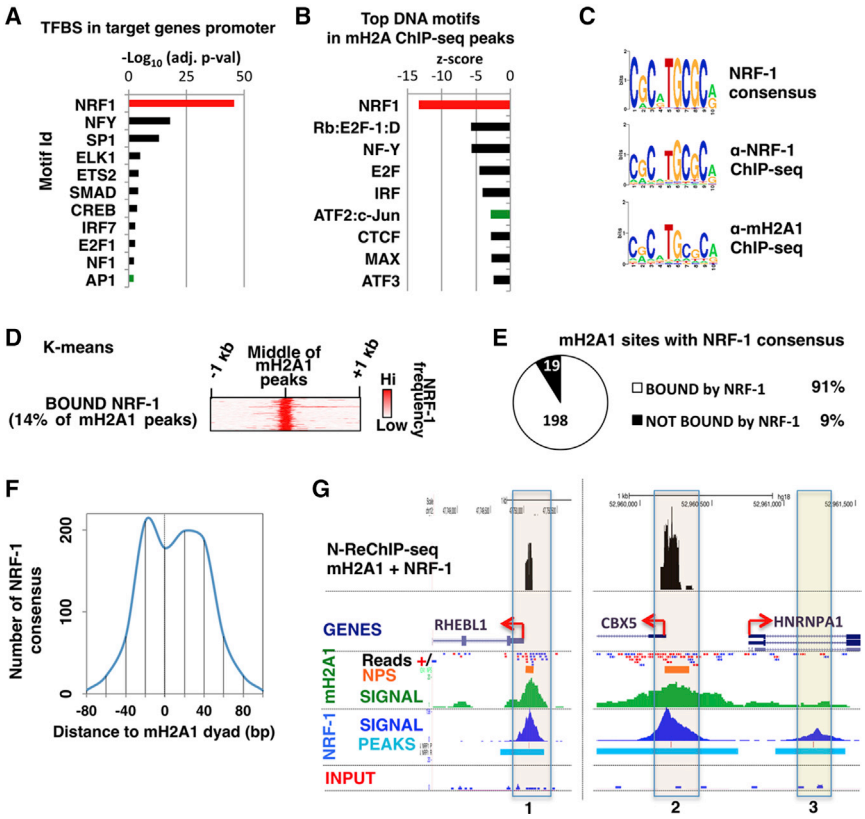

Figure 4. mH2A Nucleosomes Coexist with NRF-1

(A) Bar graph showing TFBSs enriched on gene promoters bound by mH2A in Namalwa cells (as defined in Figure 1A). Hits for TFBSs were ranked according to their probability ($-\log_{10}$ [adjusted p value]) of being found on mH2A-bound promoters.

(B) Same as in (A) except that the DNA motifs were identified in the mH2A ChIP-seq peaks for the whole genome (defined in Figure S1B, ALL PEAKS).

(C) De novo motif discovery of the NRF-1 ChIP-seq peaks. The top sequence logo depicts the known NRF-1 consensus sequence. The middle sequence logo depicts the consensus NRF-1 sequence derived from our NRF-1 ChIP-seq experiments. The bottom sequence logo depicts the best motif discovered in our mH2A ChIP-seq peaks. Note the nearly identical sequences obtained from the NRF-1 and mH2A ChIP-seq binding sites.

(D) Heatmap showing the density of NRF-1 ChIP-seq reads centered around mH2A ChIP-seq peaks (−1 kbp to +1 kbp from the middle of the peak). The darker red color indicates a higher frequency of reads. K-means clustering identified that 14% of all mH2A1 peaks are also bound by NRF-1 in their middle.

(E) Pie chart illustrating that 91% of all mH2A-bound sites containing NRF-1 consensus sequences are indeed bound by NRF-1.

(F) Plot illustrating the moving average of the number of NRF-1 consensus motifs detected in DNA sequences covered by mH2A nucleosomes (−80 bp to +100 bp to dyad axis, defined as the middle of ChIP-seq peaks).

(G) Snapshots of the genome-wide distribution of native nucleosomes containing both mH2A1 and NRF-1 as determined by N-ReChIP-seq (black track). Peaks in the density profile identified by NPS (orange bars) for mH2A1+NRF-1 co-localize with signals obtained by independent ChIP-seq analyses for mH2A1 (green track) and NRF-1 (blue track) in boxes 1 and 2. No N-ReChIP-seq peak is detected in the absence of mH2A1 ChIP-seq peak (box 3).

See also Figures S4 and S5 and Table S3.

Next, we examined whether NRF-1 and mH2A directly interact in solution and on nucleosomes. We transfected Namalwa cells with a lentiviral vector expressing myc-tagged mH2A (Supplemental Experimental Procedures) and immunoprecipitated native nucleosomes using an α-myc antibody. The precipitated nucleosomes were tested for the presence of NRF-1 by western blotting. As shown in Figure S4D, NRF-1 co-immunoprecipitates with mH2A nucleosomes, thus confirming the ChIP-seq analysis described above. In addition, we showed that mH2A and NRF-1 directly interact in solution and in the absence of DNA, and that this interaction requires the DNA binding domain (DBD) of NRF-1 and the non-histone region (NHR) of mH2A (Figure S4E).

These findings suggest that co-occupancy of NRF-1 and mH2A on relevant nucleosomes could contribute to the regulation of expression of a defined set of genes. We captured the co-occupancy state on specific promoters by carrying out native ChIP-seq of mH2A and NRF-1 followed by next-generation sequencing (N-ReChIP-seq). Native mononucleosomes were precipitated with the α-mH2A1 antibody, the bound material was eluted and then re-precipitated with the α-NRF-1 antibody, and the purified DNA was subjected to deep sequencing. Figure 4G shows a comparison of the mH2A and NRF-1 peak density profiles (green and blue, respectively) derived either from independent ChIP-seq experiments or from the N-ReChIP-seq experiment (shown in black) for the *RHEBL1* and *CBX5/HNRNPA1* promoters. The ReChIP signal is observed only in co-occupied promoters (boxes 1 and 2), and not in loci lacking mH2A1 (box 3). Additionally, control ReChIP experiments analyzed by qPCR confirmed the co-occupancy of mH2A and NRF-1 at the *DEDD2*, but not at the *COX6A1* promoter (Figure S4G).

In agreement with the data described above, K-means clustering revealed the existence of 550 gene promoters bound with high frequency by both mH2A and NRF-1 (Hi, Figure S4F). Consistent with the data described in Figure 1, we showed that double-marked nucleosomes are enriched at the promoters of both expressed and repressed genes (compare Figure S4H to Figure 1C). Importantly, we discovered that the greater the number of highly expressed genes with high-affinity mH2A nucleosomes, the higher was the probability for NRF-1 binding (Pearson correlation coefficient = 0.99; compare profiles in Figures S4I and S4J for N656). By contrast, this correlation was lower (Pearson correlation coefficient = 0.86) for the N3353 cluster containing genes bound with medium frequencies by mH2A. Overall, these results suggest that double-marked nucleosomes are preferentially enriched in promoters of highly expressed genes.

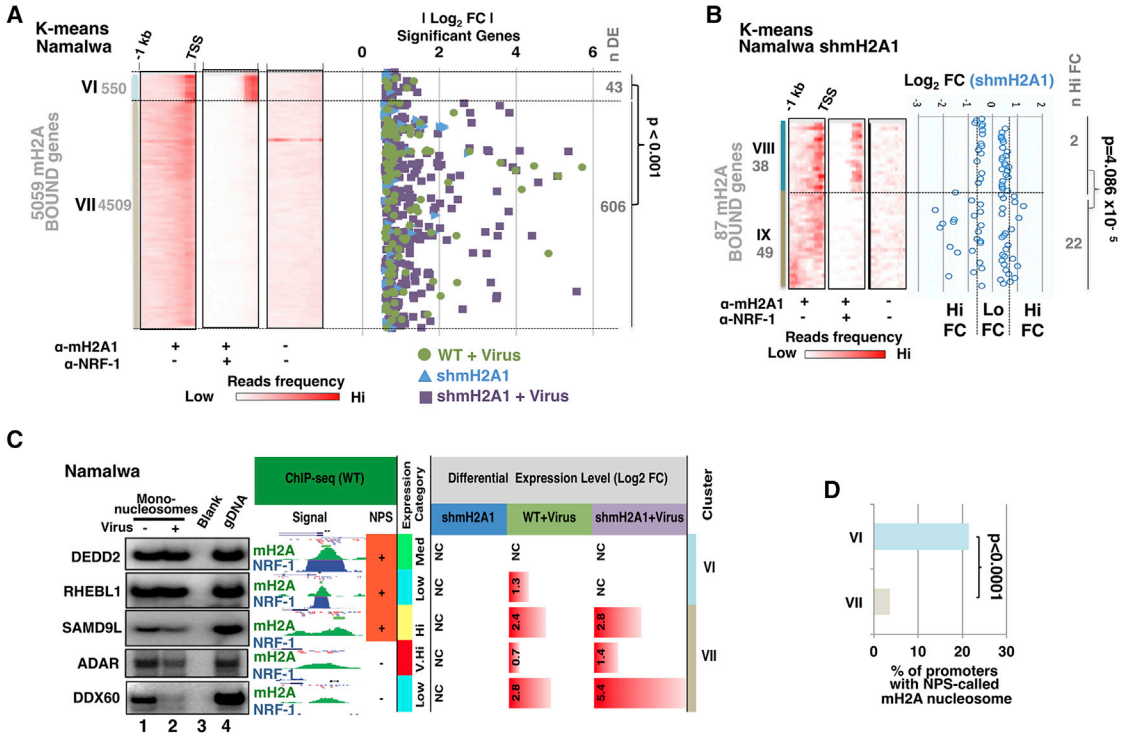

Figure 5. Stable Positioning of mH2A/NRF-1 Nucleosomes at Promoters Defines Transcriptional Robustness

(A) Heatmaps displaying K-means clustering and highlighting all promoters that are bound by mH2A1 and NRF-1 (cluster VI, 550 genes) simultaneously or by mH2A1 only (cluster VII, 4,509 genes). All mH2A1/NRF-1-containing promoters (cluster VI) are bound by mH2A1 with a higher frequency compared with mH2A only bound promoters (cluster VII). The scatterplot on the right shows the DE ($|\log_2 FC|$) of the genes after perturbation and sorted on the y axis according to K-means clustering. Green dots represent virus infection, blue triangles represent mH2A KD, and purple squares represent virus infection in mH2A KD cells. A chi-square test revealed that there are significantly more genes with DE for cluster VI than for cluster VII ($p < 0.001$).

(B) Heatmaps displaying K-means clustering and highlighting the distinct local enrichment on promoters bound by mH2A1 and NRF-1 simultaneously or by mH2A1 only, for genes with DE in Namalwa KD cells. All mH2A1/NRF-1-containing promoters (cluster VIII) are bound by mH2A1 with a higher frequency compared with mH2A-only bound promoters (cluster IX). The scatterplot on the right shows (1) the changes in the expression scores of these genes in mH2A KD Namalwa cells and (2) their correlation with the binding frequency on the same gene promoters. For both clusters, the number of genes with $|FC| > 1$ (n Hi FC) is compared with the total number of genes in the cluster. A chi-square test revealed that there are significantly more genes with Hi FC for cluster IX than for cluster VIII ($p = 4.086 \times 10^{-5}$).

(C) Direct mapping of mH2A nucleosomes. Native mononucleosomes were prepared from mock- or virus-infected Namalwa cells and the DNA was used in PCR reactions with pairs of primers corresponding to the mH2A-nucleosome-protected regions as determined by ChIP-seq analysis (see Supplemental Experimental Procedures) for the indicated genes. The ChIP-seq profiles for mH2A and NRF-1 are indicated on the right of the gel. The NPS column indicates the ability (+) or inability (−) of the NPS algorithm to detect well-positioned mH2A nucleosomes. The table at the far right shows the expression FC of the genes in WT or mH2A KD cells as indicated (NC indicates no significant changes). The expression levels of each gene as determined in WT cells (extracted from Table S4) are shown in the column labeled Expression Category.

(D) Bar graph showing a comparison of the proportion of promoters that bear well-positioned nucleosomes as defined by NPS between clusters VI and VII.

See also Figures S4–S6 and Tables S1, S2, S3, and S4.

Composite mH2A/NRF-1 Nucleosomes Define the Robustness of Antiviral Responses

Next, we investigated whether NRF-1 and mH2A work synergistically in the regulation of transcription. One possibility is that NRF-1 facilitates the recruitment of mH2A nucleosomes on specific promoters. Unfortunately, suppression of NRF-1 levels by siRNA or inducible shRNA, or overexpression of dominant-negative forms of the protein in HeLa or Namalwa cells resulted in lethality (data not shown). Thus, we could not investigate the role of NRF-1 in mH2A nucleosome positioning by a loss-of-function approach. We therefore examined the correlation between expression of genes containing the composite NRF-1/mH2A nucleosome and that of genes containing plain mH2A in mH2A KD cells. Figure 5A shows a co-clustering analysis demonstrating that among the 5,059 gene promoters bound by mH2A, the ones bearing the composite NRF-1/mH2A nucleosomes (cluster VI 550 gene promoters) are those that are bound with the highest affinity by mH2A. Most importantly, we found that these genes are resistant to alteration of their expression (i.e., with lower variability among the genes of the same cluster) after mH2A1 KD or virus infection, or a combination thereof (Figure 5A, right; chi-square test = 13.853, $p < 0.001$). By contrast, the lower-affinity mH2A-bound promoters, all of which lack NRF-1 (category VII, 4,509 genes), were more sensitive to variability in gene expression across conditions, i.e., upon genetic perturbations (mH2A KD), environmental perturbations (virus

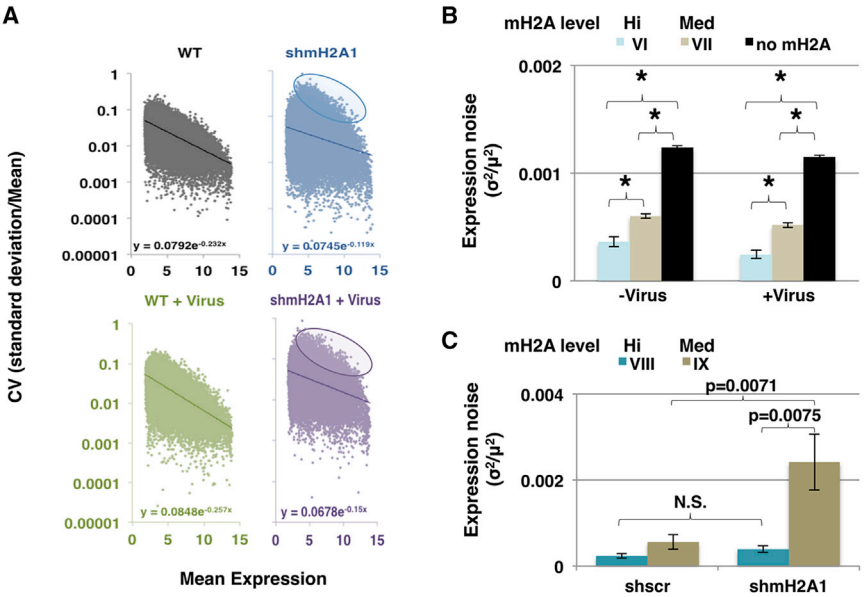

Figure 6. mH2A/NRF-1 Composite Nucleosomes Buffer Transcriptional Noise

(A) Scatterplots showing the CV of individual genes (SD/mean) against the mean of triplicates of expression intensities. Note the negative slopes indicating a negative correlation between the CV and mean expression intensity score, and the increase in CV for a subset of genes after mH2A1 KD (circled).

(B) Bar graph showing the calculated average transcriptional noise (σ^2/μ^2) ± SEM for the indicated gene clusters in mock- and virus-infected Namalwa cells (t test, *$p < 0.001$).

(C) Bar graph showing the calculated average transcriptional noise (σ^2/μ^2) ± SEM for the indicated gene clusters in control and mH2AKD Namalwa cells (p values obtained by t test are indicated; N.S. denotes $p > 0.05$).

See also Figures S2 and Tables S2 and S4.

infection), or both (Figure 5A). We obtained a similar result (Figure 5B) when we performed a reciprocal analysis. We plotted the FC expression of all mH2A target genes affected by mH2A KD and found that the genes with a lower FC were those that contained the high-affinity bound mH2A/NRF-1 nucleosomes (n = 2 and 22 genes with Hi FC in clusters VIII and IX, respectively; chi-square statistic = 16.83, $p = 4.086 \times 10^{-5}$).

To validate these observations, we carried out direct nucleosome mapping experiments on representative gene promoters bearing high- or low-affinity mH2A nucleosomes. First, we verified our ChIP-seq data by demonstrating the existence of highly positioned composite mH2A/NRF-1 nucleosomes on the promoters of the *DEDD2* and *RHEBL1* genes from cluster VI (Figure 5C). Importantly, no changes were detected in the nucleosome architecture at the *DEDD2* and *RHEBL1*, where the high-affinity, promoter-bound mH2A/NRF-1 nucleosomes remained stably bound after virus infection (Figure 5C, left, compare lanes 1 and 2). By contrast, the weakly bound mH2A nucleosomes on the promoters of the *SAMD9L*, *ADAR*, and *DDX60* genes, which lack NRF-1 (cluster VII), were destabilized upon virus infection (compare lanes 1 and 2), and this correlated with the variability of their expression upon perturbation (Figure 5C, right). Finally, we also verified that in general, the mH2A/NRF-1 composite nucleosomes (cluster VI) are more frequently well-positioned in comparison with the plain mH2A nucleosomes of cluster VII, which lack NRF-1 (Figure 5D; chi-square statistics = 299.13, $p < 0.0001$). For example, Figure S5A shows that the *POLR2H* and *ATF6B* gene promoters containing double-marked mH2A/NRF-1 nucleosomes show strong nucleosome positioning that was also identified by the NPS algorithm, whereas mH2A-nucleosomes lacking NRF-1 (e.g., *IFI44L* and *IFNA2*) show fuzzier positioning and were not identified by NPS (Figure S5B). Taken together, these data strongly suggest that NRF-1 binding correlates with high-affinity mH2A binding, thus generating stable nucleosome architectures that lead to robust regulation of gene expression and are not sensitive to genetic and/or environmental perturbations.

A prediction derived from the experiments described above is that promoter-bound mH2A nucleosomes moderate gene expression variability and, most likely, transcriptional noise between changing conditions. Recent studies have demonstrated that for multicellular organisms, one can determine transcriptional noise by calculating the normalized variation of gene expression between replicates of cell populations (Tirosh and Barkai, 2008; Yin et al., 2009; Huh et al., 2013). We hypothesized that highly stable mH2A/NRF-1 nucleosomes would limit expression noise in cell populations. To address this issue, we first verified that the coefficient of variation (CV) of expression between biological replicates is indeed negatively associated with expression abundance (Figure 6A, left column). Furthermore, KD of mH2A increased the CVs of a proportion of genes (Figure 6A, right column, circled), pointing to higher levels of noise. To verify this observation, we calculated the transcriptional noise in mH2A KD cells and/or virus-infected cells by determining the ratio σ^2/μ^2 (variance divided by the square mean of expression; see Experimental Procedures) separately for genes lacking mH2A (no mH2A) and genes bound by low- or high-affinity mH2A nucleosomes in uninfected and virus-infected cells. Figure 6B shows that genes bearing the composite mH2A/NRF-1 nucleosomes (VI-Hi mH2A) display the lowest levels of noise when compared with genes bearing plain mH2A nucleosomes (VII-Medium mH2A) in both mock and virus-infected cells (t test statistics = 3.66 and 4.15, respectively; $p < 0.001$). Importantly, genes lacking promoter-bound mH2A nucleosomes display the highest degree of transcriptional noise (Figure 6B; $p < 0.001$). Likewise, among the genes deregulated by mH2A KD, those that contain high-affinity, promoter-bound mH2A/NRF-1 nucleosomes (cluster VIII) display the lowest degree of transcriptional

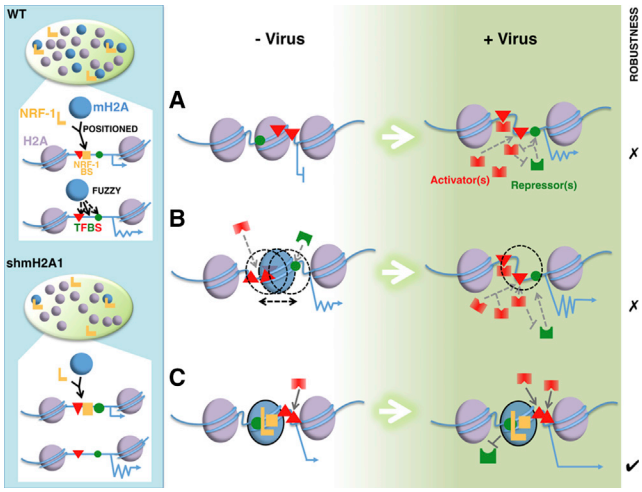

Figure 7. Model Depicting the Antagonistic Bifunctional Role of mH2A Nucleosomes in Defining Transcriptional Robustness

Shown is a model with hypothetical genes whose chromatin architecture defines specific gene expression patterns and transcriptional robustness. The left part of the figure depicts genes in WT cells where the mH2A nucleosome is positioned at specific and defined locations by NRF-1 (top) or is not accurately positioned (fuzzy) in the absence of NRF-1. The bottom part of the figure shows that in mH2A KD cells, which contain lower amounts of mH2A, NRF-1 can still recruit mH2A nucleosomes through cooperative binding interactions, thus preserving the transcriptional program. In contrast, genes bound by fuzzy mH2A nucleosomes change their expression program in KD cells.

(A) A mH2A nucleosome-free promoter, as is the case for most mH2A-independent genes, is characterized by stochastic interactions of TFs with regulatory DNA in response to virus infection, thus enhancing transcriptional noise and reducing robustness.

(B) In the absence of NRF-1, mH2A nucleosomes (shown in blue) are not stably positioned and can be evicted or slid (fuzziness, dotted ovals), especially upon perturbations. This can result in noisy expression due to the stochastic association of activators and/or repressors with the promoter and competition with remodeling complexes. Thus, variability in the binding of antagonistic transcriptional regulators can lead to transcriptional fluctuations and less robust transcriptional control of gene expression.

(C) The accurate positioning of mH2A nucleosomes by NRF-1 masks the binding site(s) for repressor(s) to their cognate binding sequences (green circle), thus allowing the activators to bind constantly to their accessible TFBS (red triangles) to activate transcription robustly. In this case, the presence of an mH2A nucleosome correlates with gene expression. The opposite could be true for another gene with masked activator binding sites, thus allowing the constant interaction of repressors with DNA to inhibit transcription. Straight blue arrows, robust transcription; wavy blue arrows, noisy transcription; dotted gray arrows, stochastic interactions; plain gray arrows, robust interactions.

noise in mH2A KD cells when compared with genes bound by plain mH2A nucleosomes (cluster IX; Figure 6C; t test statistics = 2.74; p = 0.0075). It is noteworthy that genes bound with low affinity by mH2A (cluster IX) display higher noise in mH2A KD cells than in control cells (Figure 6C; t test statistics = 2.75; p = 0.0071), whereas genes bound with high affinity by mH2A show less noise upon perturbation (cluster VIII, Figure 6C, N.S.). Taken together, these results demonstrate that the recruitment of mH2A nucleosomes and the affinity of their interaction with promoters predictably modulate transcriptional noise, thereby affecting the fate of gene expression programs.

DISCUSSION

Reliable gene expression patterns require mechanisms to minimize and/or control the inherent transcriptional noise. Here, we have shown that a specific class of mH2A nucleosomes stabilized by NRF-1 are bound with high affinity to certain promoters and reduce transcriptional noise by functioning as steady roadblocks to control the interaction of activators or repressors of transcription with their cognate sites. In general, mH2A nucleosomes work as either negative or positive regulators of transcription. We demonstrated that a solution to this apparent paradox lies in the nature of the TFBSs masked by the mH2A nucleosomes: in genes negatively regulated by mH2A, the activator binding sites are masked by mH2A nucleosomes, whereas in genes positively regulated by mH2A, the repressor binding sites are masked by mH2A nucleosomes. Thus, proper transcriptional regulation depends on the overall arrangement of specific TFBSs relative to strategically positioned mH2A nucleosomes. These context-specific effects of mH2A nucleosomes "write" specific nucleosome codes that generate a variety of transcriptional outputs by using a defined set of TFs and chromatin regulators, thereby expanding the regulatory potential of enhancers and promoters. We also uncoupled the control of gene expression noise from the ability of genes to change their expression patterns upon specific stimuli (plasticity). We anticipate that such mechanisms may influence adaptation through increased robustness (Payne and Wagner, 2014).

Decision-making within cells requires the ability to monitor environmental signals precisely and to process those signals into the appropriate actions. These actions are mediated by TF networks (Neph et al., 2012) whose inherent level of stochasticity confers a degree of unpredictability, thus promoting variability in gene expression. We reasoned that cells must have evolved ways to buffer such random variations, and here we describe a novel design of molecular interactions that ensure robust functions. The interaction between NRF-1 and mH2A nucleosomes results in a well-defined biochemical network that minimizes promoter variability, leading to stable and inheritable epigenetic landscapes that remain predictable and unchanged in response to environmental/genetic perturbations, and thus have low variability. This contradicts the anticipated effects of the impairment of chromatin organization components (Rinott et al., 2011). We argue that high-affinity mH2A-bound promoters mimic many characteristics of nucleosome-free promoters (Tirosh and Barkai, 2008; Jin et al., 2009) by displaying a constant probability of interactions with the transcriptional machinery. Furthermore, we postulate that mH2A/NRF-1 composite nucleosomes can prevent transcriptional plasticity by blocking the random access (intrusion) of "undesired" TFs, which could interfere with gene expression programs. By contrast, lower-affinity, promoter-bound mH2A nucleosomes allow the sporadic/stochastic binding of TFs followed by the recruitment (or not) of the transcriptional machinery. Thus, the promoters are constantly switched between an open and a closed state, resulting in transcriptional noise (Figure 7). We anticipate that such heterogeneity could be due to variability in the transcriptional burst size and/or frequency.

Previous studies have also reported cellular mechanisms that suppress noise. For example, miRNAs can suppress random

fluctuations in the copy number of target transcripts by feedforward or feedback loops (Ebert and Sharp, 2012; Buggele and Horvath, 2013; Ghosh et al., 2014). Chromatin remodeling factors such as HDACs can decrease the frequency or size of transcriptional bursts (Weinberger et al., 2012), whereas nucleosome-disfavoring sequences can also limit noise by allowing a fine-tuned regulation of gene expression (Raveh-Sadka et al., 2012). Finally, cell-signaling pathways are embedded with noise-suppression components (Dixit et al., 2014; Shimizu et al., 2014). Together with these previous studies, our results strongly suggest that cells have evolved various noise-suppression mechanisms that work both in parallel and antagonistically with the molecular pathways that generate noise, thus ensuring the robustness and multiplicity of the responses. These elegant biochemical counteracting pathways compensate for the inherent variability of biochemical interactions.

We have also challenged the general view that mH2A is an epigenetic repressor mark by demonstrating that plain and composite singular mH2A nucleosomes are more likely to be associated with active genes than with inactive ones (see Figure S3 and Supplemental Results). In agreement with this unexpected observation, we found that mH2A nucleosomes globally overlap with DNase hypersensitive sites and are flanked by nucleosomes containing H3K4Me3 and H2A.Z marks, all of which characterize active genes (Figures S5C and S5D).

KD of mH2A caused a dramatic change in the antiviral gene expression program, as a large number of genes that normally do not respond to virus infection (see Supplemental Results and Figure S2G, mH2A-restricted genes) were activated or repressed in mH2A KD cells. We propose that ordinarily, mH2A nucleosomes form roadblocks against the access of various constitutive and/or virus-induced TFs to gene regulatory elements (Figure 7), preventing the nearby genes from being expressed and thus defining the cell-type-specific antiviral program precisely. Indeed, a Gene Ontology (GO) analysis of abnormally expressed genes in virus-infected mH2A KD Namalwa cells (mH2A1-restricted, as defined in Supplemental Results) revealed that, in contrast to the normally activated genes (see Supplemental Results and Figure S2G, mH2A1-dependent), these genes fall into categories that are only distantly related to the antiviral response (Figure S6A). Furthermore, a motif analysis of the promoter regions revealed that mH2A-dependent, virus-induced genes in wild-type (WT) cells bear recognition sequences for IRFs and NF-kB, whereas the abnormally activated genes (mH2A-restricted) in mH2A KD cells contain a collection of binding sites for various TFs, many of which are irrelevant for virus infection (Figure S6B). The total loss or partial destabilization of mH2A nucleosomes in KD cells exposes these binding sites, thus driving the abnormal expression of the nearby genes.

This mH2A-dependent robustness against environmental fluctuations could have evolved as an adaptation to reduce the possible deleterious effects of such fluctuations and/or to serve specific functions in biological systems, such as maintaining cellular integrity in the face of various threats. Indeed, our GO analysis of the robust cluster VI revealed that it is significantly enriched for genes with "housekeeping" functions (Figure S6C, chi-square statistics = 7.956; $p = 0.0479282$; Experimental Procedures). Hence, mH2A nucleosomes may serve the major function of preserving the transcriptional stability and robustness of key genes under fluctuating conditions. Our conclusion is in agreement with recent studies in *E. coli* and yeast, which showed that changes in gene expression scale in proportion with global cellular constraints, thus reducing the degrees of freedom in changes of the expression program in response to environmental cues (Keren et al., 2013). Thus, mH2A could play a similar role in reducing or eliminating gene expression changes of mammalian genes expressed constitutively or in response to perturbations in the face of fluctuating conditions.

EXPERIMENTAL PROCEDURES

Antibodies

The antibodies used in this study were anti-mH2A1.2 (Ford et al., 2014), anti-NRF-1 (raised against full-length NRF-1 in rabbit and affinity purified from serum with recombinant NRF-1), and anti-RNApol II (AC-055-100; Diagenode).

ChIP-Seq

For N-Re-Chip, the α-mH2A1 antibody was used for the first IP, and α-NRF-1 or control IgG was used for the second round. Eluted DNA was purified using the QIAGEN Minelute PCR kit and subjected to qPCR analysis using SYBR Green (iCycler IQ; Bio-Rad Laboratories). High-throughput sequencing libraries (Illumina) were prepared according to the manufacturer's instructions. Purified libraries were sequenced on Illumina GA IIx or HiSeq2000 platforms. For additional details, see the Supplemental Experimental Procedures.

Gene Expression Analysis

DNA microarray analyses were performed as previously described (Antonaki et al., 2011) with three biological replicates on Affymetrix HG133plus2.0 chips. $FC \geq 1.5$ and $p < 0.05$ were used for DE calling, except for shmH2A1, where $FC \geq 1.3$ and $p < 0.1$ were used to detect more subtle changes. FC was calculated as such for Figure S2: +virus compares virus-infected WT cells with mock-infected WT cells, and +virus +KD compares virus-infected mH2A KD cells with virus-infected control cells treated with scramble shRNA. The DE genes are listed in Table S2. RNA-seq was performed according to the previously published strand-specific RNA-seq protocol (Parkhomchuk et al., 2009) and the libraries were sequenced on an Illumina Genome Analyzer IIx.

High-Throughput Sequencing Data Analysis

Reads were mapped to hg18 with default parameters, and uniquely aligned sequences obtained from duplicate libraries were pooled. For ChIP-seq, significantly enriched regions were identified using QuEST (Valouev et al., 2008), MACS (Zhang et al., 2008a), and SICER (Zang et al., 2009) with default parameters, and positioned nucleosomes were validated by the NPS algorithm (Zhang et al., 2008b). The intersection of the peaks obtained by MACS and QuEST was used to define sharp peaks. The relative genomic enrichment of ChIP peaks was analyzed using CEAS, and the average distribution of ChIP-seq reads around given genomic positions was calculated with Sitepro (Shin et al., 2009). Heatmaps representing K-means clustering were generated with Seqminer (Ye et al., 2011), and correlation with expression data was computed by plotting the $\log_2$ FC of the corresponding genes (see Tables S1, S3, and S4 for details regarding the reads, peaks, and clusters). Data corresponding to H3K4Me3, DNase HS, FAIRE-seq, and H2A.Z occupancy in GM12878 lymphoblastoid cells were downloaded from ENCODE (http://genome.ucsc.edu/), and data for H2A.Z and H2A.Z+H3.3 were obtained from Jin et al. (2009).

Motifs and GO Analyses

De novo motif discovery and motif matching were carried out using SeqPos (tool from Galaxy Cistrome, http://cistrome.org). GO analyses are detailed in the Supplemental Experimental Procedures. The annotation and categorization of DNA motifs enriched in up- and downregulated genes was performed as follows: first, all motifs enriched for each category of expression by Seqpos were identified on mH2A peaks defined by MACS-QuEST analysis, and then

the associated activities of TF (activators, repressors, or both) were determined from the Genecards database.

Statistical Analysis and Gene Expression Noise Estimation

For statistical analysis, p values were calculated via t test for variation of category mean values, or by chi-square test assuming a Gaussian distribution of the population to compare the number of hits per defined category. In the latter case, the null hypothesis posits that genes containing mH2A1 or mH2A1-NRF1 bound nucleosomes are distributed randomly among the tested genes. Correlations were calculated using the Pearson correlation coefficient. Analysis of expression noise in microarray data triplicates was performed on the $\log_2$-transformed normalized values using the ratio σ^2/μ^2 (variance divided by the square mean of intensities) (Raveh-Sadka et al., 2012) after it was verified that the CV (SD of triplicates divided by the mean intensities of triplicates) and expression abundance were significantly negatively correlated (Huh et al., 2013).

ACCESSION NUMBERS

The NCBI GEO accession numbers for the next-generation sequencing data and DNA microarray data reported in this paper are GEO: GSE53133 and GEO: GSE53103, respectively.

SUPPLEMENTAL INFORMATION

Supplemental Information includes Supplemental Results, Supplemental Experimental Procedures, six figures, and five tables and can be found with this article online at http://dx.doi.org/10.1016/j.celrep.2015.04.022.

ACKNOWLEDGMENTS

We thank Maria Fousteri, Darek Gorecki, Pantelis Hatzis, Stavros Lomvardas, Menie Merika, George Mosialos, George Panayotou, Paschalis Sideras, Alan Thorne, and members of D.T.'s lab for critical readings of the manuscript. We also thank Ethan Ford for the macroH2A1.1 and macroH2A1.2 antibodies. This work was supported by grants from the EU (FP6-RTN-TAF CHROMATIN, FP7-ITN-INTEGER, and FP7-NANOMA), the General Secretariat for Research and Technology (PENED 2003 and ARISTEIA I), and the KMW Offsets Program.

Received: July 9, 2014
Revised: March 6, 2015
Accepted: April 8, 2015
Published: May 7, 2015

REFERENCES

Agelopoulos, M., and Thanos, D. (2006). Epigenetic determination of a cell-specific gene expression program by ATF-2 and the histone variant macroH2A. EMBO J. *25*, 4843–4853.

Angelov, D., Molla, A., Perche, P.Y., Hans, F., Côté, J., Khochbin, S., Bouvet, P., and Dimitrov, S. (2003). The histone variant macroH2A interferes with transcription factor binding and SWI/SNF nucleosome remodeling. Mol. Cell *11*, 1033–1041.

Antonaki, A., Demetriades, C., Polyzos, A., Banos, A., Vatsellas, G., Lavigne, M.D., Apostolou, E., Mantouvalou, E., Papadopoulou, D., Mosialos, G., and Thanos, D. (2011). Genomic analysis reveals a novel nuclear factor-κB (NF-κB)-binding site in Alu-repetitive elements. J. Biol. Chem. *286*, 38768–38782.

Barkai, N., and Shilo, B.-Z. (2007). Variability and robustness in biomolecular systems. Mol. Cell *28*, 755–760.

Barrero, M.J., Sese, B., Kuebler, B., Bilic, J., Boue, S., Martí, M., and Izpisua Belmonte, J.C. (2013). Macrohistone variants preserve cell identity by preventing the gain of H3K4me2 during reprogramming to pluripotency. Cell Rep. *3*, 1005–1011.

Boulard, M., Storck, S., Cong, R., Pinto, R., Delage, H., and Bouvet, P. (2010). Histone variant macroH2A1 deletion in mice causes female-specific steatosis. Epigenetics Chromatin *3*, 8.

Buggele, W.A., and Horvath, C.M. (2013). MicroRNA profiling of Sendai virus-infected A549 cells identifies miR-203 as an interferon-inducible regulator of IFIT1/ISG56. J. Virol. *87*, 9260–9270.

Buschbeck, M., Uribesalgo, I., Wibowo, I., Rué, P., Martin, D., Gutierrez, A., Morey, L., Guigó, R., López-Schier, H., and Di Croce, L. (2009). The histone variant macroH2A is an epigenetic regulator of key developmental genes. Nat. Struct. Mol. Biol. *16*, 1074–1079.

Cairns, B.R. (2009). The logic of chromatin architecture and remodelling at promoters. Nature *461*, 193–198.

Campos, E.I., and Reinberg, D. (2009). Histones: annotating chromatin. Annu. Rev. Genet. *43*, 559–599.

Chakravarthy, S., Gundimella, S.K.Y., Caron, C., Perche, P.Y., Pehrson, J.R., Khochbin, S., and Luger, K. (2005). Structural characterization of the histone variant macroH2A. Mol. Cell. Biol. *25*, 7616–7624.

Changolkar, L.N., Singh, G., Cui, K., Berletch, J.B., Zhao, K., Disteche, C.M., and Pehrson, J.R. (2010). Genome-wide distribution of macroH2A1 histone variants in mouse liver chromatin. Mol. Cell. Biol. *30*, 5473–5483.

Cheung, D., Miles, C., Kreitman, M., and Ma, J. (2014). Adaptation of the length scale and amplitude of the Bicoid gradient profile to achieve robust patterning in abnormally large Drosophila melanogaster embryos. Development *141*, 124–135.

Choi, J.K., and Kim, Y.-J. (2009). Intrinsic variability of gene expression encoded in nucleosome positioning sequences. Nat. Genet. *41*, 498–503.

Costanzi, C., and Pehrson, J.R. (1998). Histone macroH2A1 is concentrated in the inactive X chromosome of female mammals. Nature *393*, 599–601.

Dixit, G., Kelley, J.B., Houser, J.R., Elston, T.C., and Dohlman, H.G. (2014). Cellular noise suppression by the regulator of G protein signaling Sst2. Mol. Cell *55*, 85–96.

Ebert, M.S., and Sharp, P.A. (2012). Roles for microRNAs in conferring robustness to biological processes. Cell *149*, 515–524.

Evans, M.J., and Scarpulla, R.C. (1990). NRF-1: a trans-activator of nuclear-encoded respiratory genes in animal cells. Genes Dev. *4*, 1023–1034.

Ford, E., Nikopoulou, C., Kokkalis, A., and Thanos, D. (2014). A method for generating highly multiplexed ChIP-seq libraries. BMC Res. Notes *7*, 312.

Gamble, M.J., Frizzell, K.M., Yang, C., Krishnakumar, R., and Kraus, W.L. (2010). The histone variant macroH2A1 marks repressed autosomal chromatin, but protects a subset of its target genes from silencing. Genes Dev. *24*, 21–32.

Gaspar-Maia, A., Qadeer, Z.A., Hasson, D., Ratnakumar, K., Leu, N.A., Leroy, G., Liu, S., Costanzi, C., Valle-Garcia, D., Schaniel, C., et al. (2013). MacroH2A histone variants act as a barrier upon reprogramming towards pluripotency. Nat. Commun. *4*, 1565.

Ghosh, T., Aprea, J., Nardelli, J., Engel, H., Selinger, C., Mombereau, C., Lemonnier, T., Moutkine, I., Schwendimann, L., Dori, M., et al. (2014). MicroRNAs establish robustness and adaptability of a critical gene network to regulate progenitor fate decisions during cortical neurogenesis. Cell Rep. *7*, 1779–1788.

Huh, I., Zeng, J., Park, T., and Yi, S.V. (2013). DNA methylation and transcriptional noise. Epigenetics Chromatin *6*, 9.

Iyer, V.R. (2012). Nucleosome positioning: bringing order to the eukaryotic genome. Trends Cell Biol. *22*, 250–256.

Jiang, C., and Pugh, B.F. (2009). Nucleosome positioning and gene regulation: advances through genomics. Nat. Rev. Genet. *10*, 161–172.

Jin, C., Zang, C., Wei, G., Cui, K., Peng, W., Zhao, K., and Felsenfeld, G. (2009). H3.3/H2A.Z double variant-containing nucleosomes mark 'nucleosome-free regions' of active promoters and other regulatory regions. Nat. Genet. *41*, 941–945.

Kapoor, A., Goldberg, M.S., Cumberland, L.K., Ratnakumar, K., Segura, M.F., Emanuel, P.O., Menendez, S., Vardabasso, C., Leroy, G., Vidal, C.I., et al.

(2010). The histone variant macroH2A suppresses melanoma progression through regulation of CDK8. Nature *468*, 1105–1109.

Keren, L., Zackay, O., Lotan-Pompan, M., Barenholz, U., Dekel, E., Sasson, V., Aidelberg, G., Bren, A., Zeevi, D., Weinberger, A., et al. (2013). Promoters maintain their relative activity levels under different growth conditions. Mol. Syst. Biol. *9*, 701.

Li, Z., Gadue, P., Chen, K., Jiao, Y., Tuteja, G., Schug, J., Li, W., and Kaestner, K.H. (2012). Foxa2 and H2A.Z mediate nucleosome depletion during embryonic stem cell differentiation. Cell *151*, 1608–1616.

Luger, K., Dechassa, M.L., and Tremethick, D.J. (2012). New insights into nucleosome and chromatin structure: an ordered state or a disordered affair? Nat. Rev. Mol. Cell Biol. *13*, 436–447.

Neph, S., Stergachis, A.B., Reynolds, A., Sandstrom, R., Borenstein, E., and Stamatoyannopoulos, J.A. (2012). Circuitry and dynamics of human transcription factor regulatory networks. Cell *150*, 1274–1286.

Parkhomchuk, D., Borodina, T., Amstislavskiy, V., Banaru, M., Hallen, L., Krobitsch, S., Lehrach, H., and Soldatov, A. (2009). Transcriptome analysis by strand-specific sequencing of complementary DNA. Nucleic Acids Res. *37*, e123.

Pasque, V., Gillich, A., Garrett, N., and Gurdon, J.B. (2011). Histone variant macroH2A confers resistance to nuclear reprogramming. EMBO J. *30*, 2373–2387.

Payne, J.L., and Wagner, A. (2014). The robustness and evolvability of transcription factor binding sites. Science *343*, 875–877.

Pehrson, J.R., and Fried, V.A. (1992). MacroH2A, a core histone containing a large nonhistone region. Science *257*, 1398–1400.

Raser, J.M., and O'Shea, E.K. (2005). Noise in gene expression: origins, consequences, and control. Science *309*, 2010–2013.

Raveh-Sadka, T., Levo, M., Shabi, U., Shany, B., Keren, L., Lotan-Pompan, M., Zeevi, D., Sharon, E., Weinberger, A., and Segal, E. (2012). Manipulating nucleosome disfavoring sequences allows fine-tune regulation of gene expression in yeast. Nat. Genet. *44*, 743–750.

Rinott, R., Jaimovich, A., and Friedman, N. (2011). Exploring transcription regulation through cell-to-cell variability. Proc. Natl. Acad. Sci. USA *108*, 6329–6334.

Sadeh, R., and Allis, C.D. (2011). Genome-wide "re"-modeling of nucleosome positions. Cell *147*, 263–266.

Sanchez, A., Choubey, S., and Kondev, J. (2013). Regulation of noise in gene expression. Annu. Rev. Biophys. *42*, 469–491.

Schones, D.E., Cui, K., Cuddapah, S., Roh, T.-Y., Barski, A., Wang, Z., Wei, G., and Zhao, K. (2008). Dynamic regulation of nucleosome positioning in the human genome. Cell *132*, 887–898.

Shimizu, H., Woodcock, S.A., Wilkin, M.B., Trubenová, B., Monk, N.A.M., and Baron, M. (2014). Compensatory flux changes within an endocytic trafficking network maintain thermal robustness of Notch signaling. Cell *157*, 1160–1174.

Shin, H., Liu, T., Manrai, A.K., and Liu, X.S. (2009). CEAS: cis-regulatory element annotation system. Bioinformatics *25*, 2605–2606.

Spitz, F., and Furlong, E.E.M. (2012). Transcription factors: from enhancer binding to developmental control. Nat. Rev. Genet. *13*, 613–626.

Struhl, K., and Segal, E. (2013). Determinants of nucleosome positioning. Nat. Struct. Mol. Biol. *20*, 267–273.

Sunadome, K., Suzuki, T., Usui, M., Ashida, Y., and Nishida, E. (2014). Antagonism between the master regulators of differentiation ensures the discreteness and robustness of cell fates. Mol. Cell *54*, 526–535.

Talbert, P.B., and Henikoff, S. (2010). Histone variants—ancient wrap artists of the epigenome. Nat. Rev. Mol. Cell Biol. *11*, 264–275.

Tanasijevic, B., and Rasmussen, T.P. (2011). X chromosome inactivation and differentiation occur readily in ES cells doubly-deficient for macroH2A1 and macroH2A2. PLoS ONE *6*, e21512.

Tirosh, I., and Barkai, N. (2008). Two strategies for gene regulation by promoter nucleosomes. Genome Res. *18*, 1084–1091.

Umlauf, D., Goto, Y., and Feil, R. (2004). Site-specific analysis of histone methylation and acetylation. In Epigenetics Protocols, T. Tollefsbol, ed. (Humana Press), pp. 99–120.

Valouev, A., Johnson, D.S., Sundquist, A., Medina, C., Anton, E., Batzoglou, S., Myers, R.M., and Sidow, A. (2008). Genome-wide analysis of transcription factor binding sites based on ChIP-Seq data. Nat. Methods *5*, 829–834.

Virbasius, C.A., Virbasius, J.V., and Scarpulla, R.C. (1993). NRF-1, an activator involved in nuclear-mitochondrial interactions, utilizes a new DNA-binding domain conserved in a family of developmental regulators. Genes Dev. *7* (*12A*), 2431–2445.

Wang, X., Bai, L., Bryant, G.O., and Ptashne, M. (2011). Nucleosomes and the accessibility problem. Trends Genet. *27*, 487–492.

Weinberger, L., Voichek, Y., Tirosh, I., Hornung, G., Amit, I., and Barkai, N. (2012). Expression noise and acetylation profiles distinguish HDAC functions. Mol. Cell *47*, 193–202.

Ye, T., Krebs, A.R., Choukrallah, M.-A., Keime, C., Plewniak, F., Davidson, I., and Tora, L. (2011). seqMINER: an integrated ChIP-seq data interpretation platform. Nucleic Acids Res. *39*, e35.

Yin, S., Wang, P., Deng, W., Zheng, H., Hu, L., Hurst, L.D., and Kong, X. (2009). Dosage compensation on the active X chromosome minimizes transcriptional noise of X-linked genes in mammals. Genome Biol. *10*, R74.

Zang, C., Schones, D.E., Zeng, C., Cui, K., Zhao, K., and Peng, W. (2009). A clustering approach for identification of enriched domains from histone modification ChIP-Seq data. Bioinformatics *25*, 1952–1958.

Zhang, Z., and Pugh, B.F. (2011). High-resolution genome-wide mapping of the primary structure of chromatin. Cell *144*, 175–186.

Zhang, Y., Liu, T., Meyer, C.A., Eeckhoute, J., Johnson, D.S., Bernstein, B.E., Nusbaum, C., Myers, R.M., Brown, M., Li, W., and Liu, X.S. (2008a). Model-based analysis of ChIP-Seq (MACS). Genome Biol. *9*, R137.

Zhang, Y., Shin, H., Song, J.S., Lei, Y., and Liu, X.S. (2008b). Identifying positioned nucleosomes with epigenetic marks in human from ChIP-Seq. BMC Genomics *9*, 537.